Cell Nuclei and Cytoplasm Joint Segmentation Using the Sliding Band Filter

Pedro Quelhas*, *Member, IEEE*, Monica Marcuzzo, Ana Maria Mendonça, *Senior Member, IEEE*, and Aurélio Campilho, *Member, IEEE*

***Abstract*—Microscopy cell image analysis is a fundamental tool for biological research. In particular, multivariate fluorescence microscopy is used to observe different aspects of cells in cultures. It is still common practice to perform analysis tasks by visual inspection of individual cells which is time consuming, exhausting and prone to induce subjective bias. This makes automatic cell image analysis essential for large scale, objective studies of cell cultures. Traditionally the task of automatic cell analysis is approached through the use of image segmentation methods for extraction of cells' locations and shapes. Image segmentation, although fundamental, is neither an easy task in computer vision nor is it robust to image quality changes. This makes image segmentation for cell detection semi-automated requiring frequent tuning of parameters. We introduce a new approach for cell detection and shape estimation in multivariate images based on the sliding band filter (SBF). This filter's design makes it adequate to detect overall convex shapes and as such it performs well for cell detection. Furthermore, the parameters involved are intuitive as they are directly related to the expected cell size. Using the SBF filter we detect cells' nucleus and cytoplasm location and shapes. Based on the assumption that each cell has the same approximate shape center in both nuclei and cytoplasm fluorescence channels, we guide cytoplasm shape estimation by the nuclear detections improving performance and reducing errors. Then we validate cell detection by gathering evidence from nuclei and cytoplasm channels. Additionally, we include overlap correction and shape regularization steps which further improve the estimated cell shapes. The approach is evaluated using two datasets with different types of data: a 20 images benchmark set of simulated cell culture images, containing 1000 simulated cells; a 16 images Drosophila melanogaster Kc167 dataset containing 1255 cells, stained for DNA and actin. Both image datasets present a difficult problem due to the high variability of cell shapes and frequent cluster overlap between cells. On the Drosophila dataset our approach achieved a precision/recall of 95%/69% and 82%/90% for nuclei and cytoplasm detection respectively and an overall accuracy of 76%.**

***Index Terms*—Cell segmentation, convergence filters, image processing in biology, multivariate image processing.**

Manuscript received February 05, 2010; revised March 30, 2010; accepted March 30, 2010. Date of publication June 03, 2010; date of current version August 04, 2010. This work was supported by Fundação para a Ciência e Tecnologia, under contract ERA-PG/0007/2006. *Asterisk indicates corresponding author.*

*P. Quelhas is with the Instituto de Engenharia Biomédica (INEB), 4200-465 Porto, Portugal (e-mail: pedro.quelhas@gmail.com).

M. Marcuzzo is with the Instituto de Engenharia Biomédica (INEB), 4200-465 Porto, Portugal.

A. M. Mendonça, and A. Campilho are with the Instituto de Engenharia Biomédica (INEB), 4200-465 Porto, Portugal and also with the Faculdade de Engenharia, Universidade do Porto, 4200-465 Porto, Portugal.

Color versions of one or more of the figures in this paper are available online at http://ieeexplore.ieee.org.

Digital Object Identifier 10.1109/TMI.2010.2048253

I. Introduction

MUCH of cell biology experimental research is based on microscopy image analysis of cell culture. In many cases the use of different fluorescence dies or proteins is used to enable the collection of multivariate images which contain information on different aspects of each cell. Although analysis of such images can be performed manually, it is time consuming, exhausting and prone to human error, requiring frequent repetitions to validate results. These factors motivate the development of automatic cell analysis tools, to identify each individual cell and extract relevant cell characteristics. This process involves the separation of each individual cell from all others cells and from the background [6], [28].

Multivariate imaging is widely used in cell microscopy to obtain separated cell nucleus and cytoplasm information by using different fluorescence markers, originating two image channels. Additional fluorescence markers (and channels) can be used to express other phenomena or objects such as parasites or different nucleic acid concentrations.

The classic methodology for cell detection is image segmentation, which is a fundamental and difficult problem in computer vision. When there is a high contrast between cells and background, the detection task can be solved by image thresholding [9], [25], applied independently to all channels and then merged using spatial dependencies. However, this approach is not able to discriminate touching cells, as the spatial relations are not embedded in basic thresholding techniques. A common alternative to image thresholding is the watershed transform, which can segment touching objects as long as separate initializing seeds can be found. Watershed methods, when used in multivariate images, use nuclei location information to seed the process for cytoplasm segmentation [25], [26]. This is motivated by the common good discrimination of the nuclei from the background and overall higher pixel contrast when compared with the cytoplasm channel. One drawback of watershed based segmentation is over-segmentation, due to the frequent presence of multiple markers per object resulting from a poor or inadequate initialization. There are two approaches to address the watershed's over-segmentation: fragment merging and marker-controlled watershed [1], [13]. None of these approaches analyzes jointly all available spectral information. Other approaches take into account the concavities in segmented shapes and assume those to indicate that such shape is a cluster of cells [3]. Clusters are subsequently split based on the location of concavities. Graph-cut methods have also been applied to cell segmentation, facing the same problem of separating cell clusters which are dealt with by introducing shape priors [4]. Additionally, other approaches have been formulated by assuming strong prior on cell shape

as circular or ellipsoidal shape. Radon or Hough transforms together with morphological processing of the thresholded image are used for this purpose [5], [23].

A more robust family of approaches to the cell detection problem is the family of deformable models, which consist in finding the boundaries of the object of interest by evolving contours or surfaces guided by internal and external forces [16]. Several deformable models methods for cell segmentation have been proposed where, starting from an initial nuclei contour, a final cytoplasm contour is adapted based on cytoplasm fluorescence evidence and cell shape priors [2], [8], [27]. When no nuclei information is available, a Voronoi diagram can be employed to construct initial contour shapes [10]. Since the traditional deformable models depend on several parameters, it is difficult to design a strategy with generalization ability to work for all images. Also, the final result is very dependent on the initial guess which is still based on the initial segmentation. Consequently, to achieve a satisfactory solution, the initial guess should be sufficiently close to the boundaries of interest which may not be possible for all cases. In recent years, deformable models based on level sets have become increasingly popular because they neither require any explicit parametrization nor suffer from any topology constraints [22], [25]. However, these still suffer from dependency on finding starting nuclei shapes to define the number of cells in each image, and their respective positions.

Although the aforementioned methods are reasonably successful on each of the specific application for which they have been designed, they still depend on several preprocessing steps and make the final detection of cells highly dependent on initial parameters which must be set by someone with image processing knowledge.

One of the main problems in any of the mentioned segmentation methods is that contrast and noise conditions must be evaluated and taken into account before segmentation, as the method's parameters are not robust to such conditions. We propose the use of the sliding band filter (SBF) [18], [19] for cell detection in multivariate microscopy images. Being a convergence filter, the SBF is fundamentally well suited for cell detection as cells have an overall convex shape. Within the field of cell detection it has already proven to perform well in low contrast and noisy single channel cell detection applications [14], [15], [20]. The SBF filter is based on gradient convergence and not intensity and as such can detect low contrast cell information which otherwise would be lost in the background noise. Additionally, the convergence evaluation in a regional band allows the reduction of uncertainty caused by noise. As an additional advantage, the SBF filter's parameters are directly related to simple observable image characteristics like cell size and shape, leading to an easy setup of parameters even by someone with no knowledge of the underlying image processing details.

To apply the SBF filter to multivariate images we assume that the gradient convergence center of the cell's nuclei and cytoplasm images is the same. This enables the use of nuclei detection information to guide the cytoplasm shape segmentation, and by doing so we are able to avoid errors caused by noise in the images. Contrary to state of the art methods like active contours, this approach constrains the final shape, limiting unlikely shape estimation deviations. Using the same assumption, we propose a detection criteria that jointly evaluates the nuclei and cytoplasm convergence for the estimated cell center and removes cell detections which do not meet a minimum convergence level. In this way errors in nuclei detection do not imply an erroneous final cell detection.

To limit the allowed cell shape and cell overlap in the final cell detection results, we introduce two correction steps. First, overlap is corrected by assuming that cells' highly irregular cytoplasm shapes that greatly overlap other cells were incorrectly estimated. Second, cell shapes are regularized to eliminate strong discontinuities. This is performed using radial smoothness and gradient convergence as the internal and external energies are embedded in the regularization of the shapes. While the use of radial coordinates for active contour in the task of cell segmentation has already been introduced [8], the joint use of radial active contours and convergence as the external energy for such contour is novel.

This paper is organized as follows. Section II introduces the data used in our experiments. Section III describes our approach for cell segmentation based on the sliding band convergence filter and Section IV presents the results obtained. Finally, the conclusion is derived in Section V.

II. Image Acquisition and Simulation

To evaluate the use of the SBF filter for cell segmentation in multivariate microscopy images we use two distinct datasets of cell culture images.

1) Drosophila Kc167 Dataset: containing 1255 Drosophila Kc167 cells, where cells were stained for DNA (to label nuclei) and actin (a cytoskeletal protein, to show the cell body) [9]. Images were acquired using a motorized Zeiss Axioplan 2 and a Axiocam MRm camera, and are provided courtesy of the laboratory of David Sabatini at the Whitehead Institute for Biomedical Research. Each image has a size that varies between 400×400 and 512×512 pixels, with cells of approximately 25 pixels in diameter, and an average of 80 cells per image. The two channels (DNA and actin) of each image are stored in separate gray-scale 8-bit TIFF files.[1] Fig. 1 shows two examples in the dataset and the corresponding groundtruth contours. We selected this image dataset as it presents an interesting level of challenge in a multivariate cell detection task. In this type of cell images not even the nuclei segmentation is considered a trivial matter [25]. However, it is the cytoplasm segmentation that poses a more complex segmentation problem [9], [25].

2) Simulated Cell Culture Dataset: containing 20 cell culture synthetic images, with 1000 simulated cells, designed for the validation of cell image analysis algorithms. With this simulator it is possible to control the cell culture population properties and microscope acquisition.[2] [12] Each image has a size of 950×950 pixels. Acquisition parameters include spatially variable out-of-focus blurring, irregular illumination variations and sensor noise. Although the selection of the many cell culture and acquisition simulation parameters is possible, we follow the settings suggested by the simulator developers [21], using

[1]Available at http://www.broadinstitute.org/bbbc/drosophila_kc167_2.html

[2]Available at http://www.cs.tut.fi/sgn/csb/simcep/benchmark/.

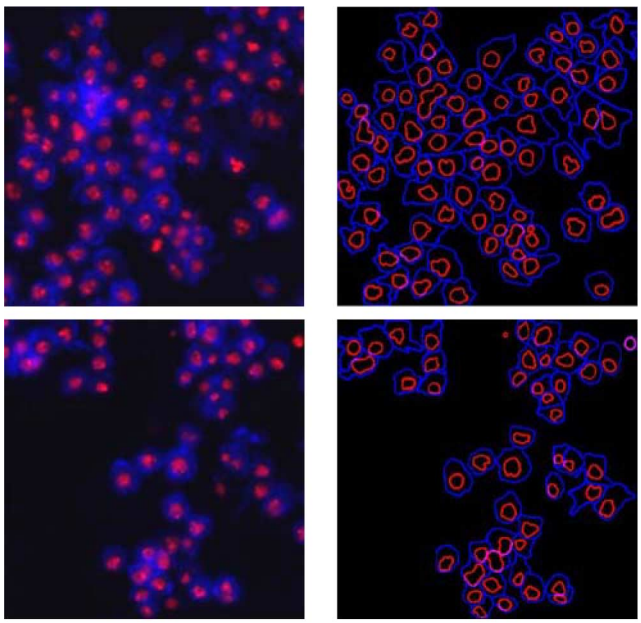

Fig. 1. Examples of microscopy images from the Drosophila melanogaster Kc167 dataset. Left: nuclei (red) and cytoplasm (blue) false color fluorescence images; right: nuclei (red) and cytoplasm (blue) groundtruth contours (available at http://www.broadinstitute.org/bbbc/drosophila_kc167_2.html). The image contrast was enhanced by 30% for better printing and display quality.

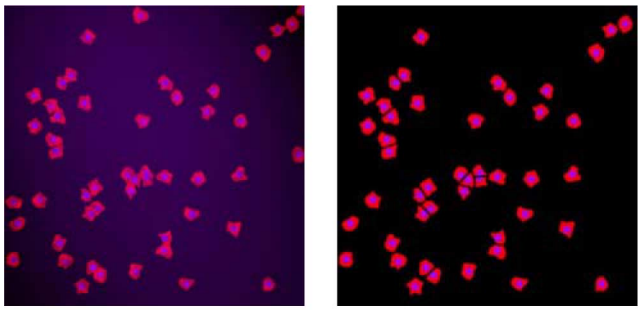

Fig. 2. Examples of simulated cell culture images (left) and corresponding groundtruth (right), where nuclei are visible in the blue channel and cytoplasm in red. Clustering and overlap of cells can be observed. These cells were generated according to the methodology introduced by Lehmussola *et al.* [12] (available at http://www.cs.tut.fi/sgn/csb/simcep/benchmark/).

50 cell per image, a 0.25 probability of clustering and allowing for overlap. Fig. 2 shows an example of the images in this dataset and corresponding available groundtruth.

The images in both datasets present a difficult problem due to the high variability of cell shapes and frequent overlap between cells. However, our approach is not specific for these images and could be applied to other multivariate cell images.

III. Methodology

Our approach to cell detection in multivariate microscopy images is based on local image filtering using the SBF filter. As most previous work on multivariate cell segmentation, we will approach nuclei and cytoplasm information separately in an initial step, starting by detecting potential nuclei. From the detected nuclei we estimate the cells' cytoplasm shapes, followed

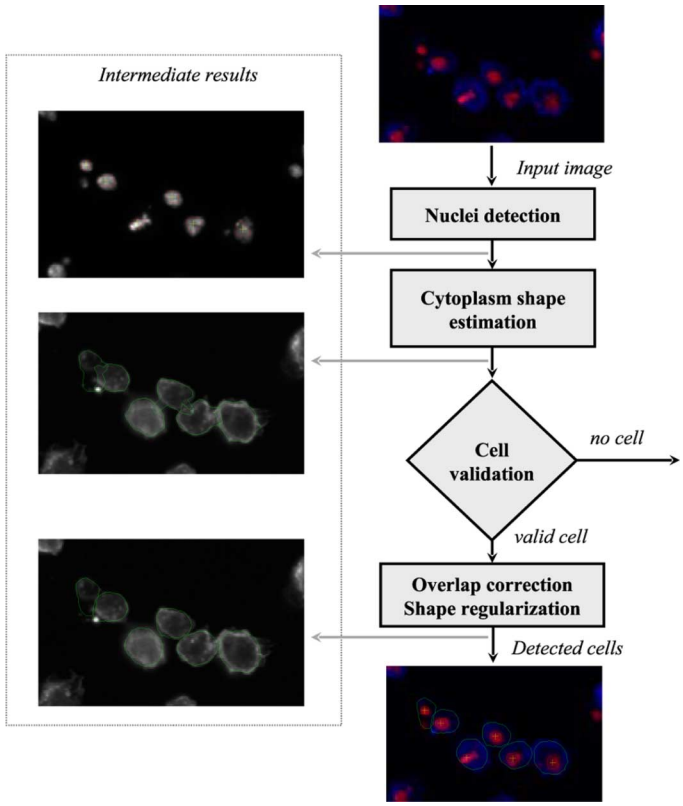

Fig. 3. Cell detection diagram, using example images from the Drosophila Kc167 dataset illustrating our approach. Images relating to nuclei and cytoplasm shape estimation show only the respective fluorescence channel.

by overlap correction and shape regularization. Fig. 3 shows the different steps used in this approach, together with example images from the Drosophila Kc167 dataset. Nuclei detection is only considered as final when there is enough evidence of a valid corresponding cytoplasm detection.

We approach the task of cell nuclei segmentation as one of local image enhancement through filtering, where locations corresponding to cell nuclei will have a strong filter response. Subsequently, cell nuclei are tentatively associated with the locations of filter maxima response.

Given the nuclei locations we estimate the nuclei shape and the corresponding cytoplasm detection, leading to a tentative detection of a cell. The estimation of the cell's cytoplasm shape is based on the assumption that the gradient convergence center of the cell's nuclei and cytoplasm image channels is the same, making the approach less sensitive to non convergent (noisy) gradient image information. The detection's validity is evaluated based on the gradient convergence evidence from both nuclei and cytoplasm images, eliminating partial errors in the detection of nuclei.

After cell detection validation, we analyze and correct cell overlap and perform shape regularization. This leads to the final result of our approach.

In Sections III-A–III-D, we will first introduce the cell nuclei detection based on the SBF filter followed by the description of the cytoplasm shape estimation. Our methodology will end with several steps to improve the final detection by reducing cell overlap and regularizing cell shape.

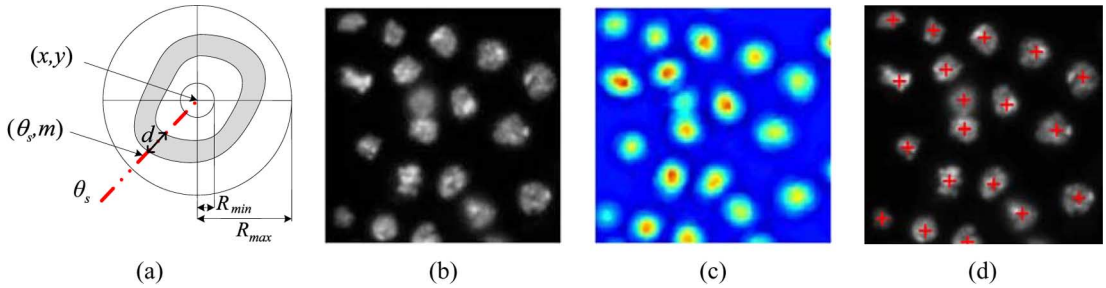

Fig. 4. SBF: (a) support region schematics; (b) original cell nuclei image; (c) filter response magnitude image; (d) cell nuclei detections overlaid on the original image.

A. Cell Nuclei Detection

The classic approach to cell nuclei segmentation is usually based on an intensity thresholding method [6], [7], [9], [25]. The use of such simple methods for this segmentation task is sometimes justified by the overall good spatial separation of cell nuclei and relatively high contrast. However, most of those solutions require a considerable amount of preprocessing steps in order to overcome issues like irregular illumination, channel cross-talk and noise [6], [7], [25].

Our approach to nuclei detection is based on highlighting image locations that exhibit characteristics indicating the presence of a nucleus, through local filtering. Since nuclei have overall convex shape, a filter from the convergence index filter family [11] was selected to perform this enhancement task. Convergence index (CI) filters are based on the maximization of the convergence index at each image point of spatial coordinates (x, y), defined by

$$C(x,y) = \frac{1}{M} \sum_{(k,l)\in R} \cos\theta(k,l) \tag{1}$$

where M is the number of points in the filter support region R, θ is the angle between the gradient vector calculated at point (k, l) and the direction of the line that connects points (x, y) and (k, l).

The main difference between the distinct members of the CI family is the definition of the support region R, where convergence is estimated. Several CI filters have been proposed: coin filter (CF), iris filter (IF), adaptive ring filter (ARF) [11], [24], and the more recent sliding band filter (SBF) [18]. The CF uses a circle with variable radius as support region, the IF maximizes the convergence index by adapting the circle's radius value on each direction and the ARF uses a ring shaped region with fixed width and varying radius. Finally, the SBF combines the ideas of IF and ARF by defining a support region formed by a band of fixed width, whose position is changed in each direction to allow the maximization of the convergence index at each point, as depicted in Fig. 4(a). When compared with the other members of the CI family the more generic formulation of the SBF gives a wider detection range of shapes in comparison with other convergence filters. This is desirable for our application due to possible cell nuclei shape variations. Additionally, the SBF bases its detection on a narrow band and ignores the gradient information at the center of the nuclei that may sometimes be noisy and irrelevant for shape estimation. The SBF filter is defined as

$$\mathrm{SBF}(x,y) = \frac{1}{N}\sum_{s=1}^{N} \max_{R^n_{\min}\le r\le R^n_{\max}} \times \left(\frac{1}{d+1}\sum_{m=r-(d/2)}^{r+(d/2)} CI(s,m)\right) \tag{2}$$

with

$$CI(s,m) = \cos(\theta_s - \alpha(\theta_s,m))$$
$$\theta_s = \frac{2\pi}{N}(s-1)$$
$$\alpha(\theta_s,m) = \arctan\left(\frac{\frac{dI^n(\theta_s,m)}{dx}}{\frac{dI^n(\theta_s,m)}{dy}}\right)$$

where I^n is the input nuclei image channel, N is the number of support region lines that irradiate from (x, y), d is the band width, r is the position of the band in a line that varies from $R^n_{\min}$ to $R^n_{\max}$, and $\cos(\theta_s - \alpha(\theta_s, m))$ is the cosine of the angle between the direction that is currently being analyzed θ_s and the image gradient vector direction at location (θ_s, m) (Fig. 4(a) shows the filter design schematics).

Equation (2) provides an estimate of the value of the gradient convergence for each image position. However, we can speed up the cell detection process by ignoring areas with no gradient information. From the SBF filter response map [Fig. 4(c)], cell nuclei are associated with the locations of filter maxima response, above a given threshold. The maxima are obtained by non-maxima suppression filtering [Fig. 4(d)].

Given the detected cell nuclei center coordinates, we can estimate their shapes in order to complete the cell nuclei detection. Based on SBF convergence filter approach used for nuclei detection we inspect the position of the band that maximizes the convergence index response in each direction of the SBF region of support. Those maximum convergence locations give an indication of the nucleus border localization. To estimate the nuclei shape we search, for each nuclei detection, which were the positions of the sliding band (band support points)

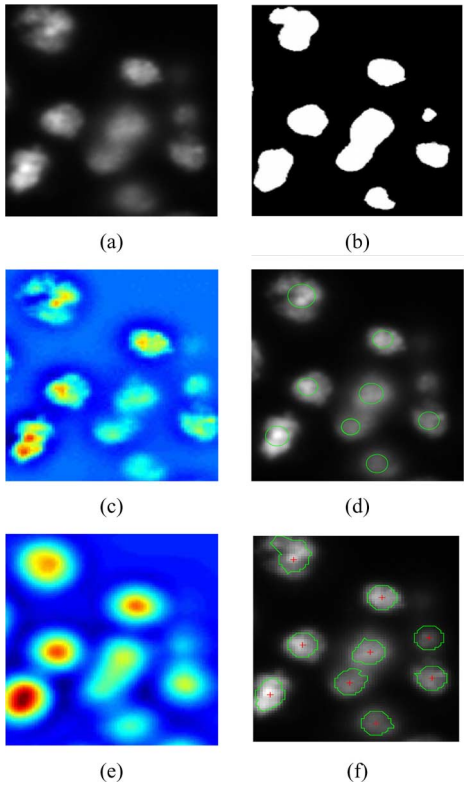

Fig. 5. Drosophila Kc167 dataset cell nuclei detection and shape estimation comparison between the Otsu segmentation method (b), the Laplacian of Gaussian (LoG) multiscale local point detector (d), and the SBF filter (f).

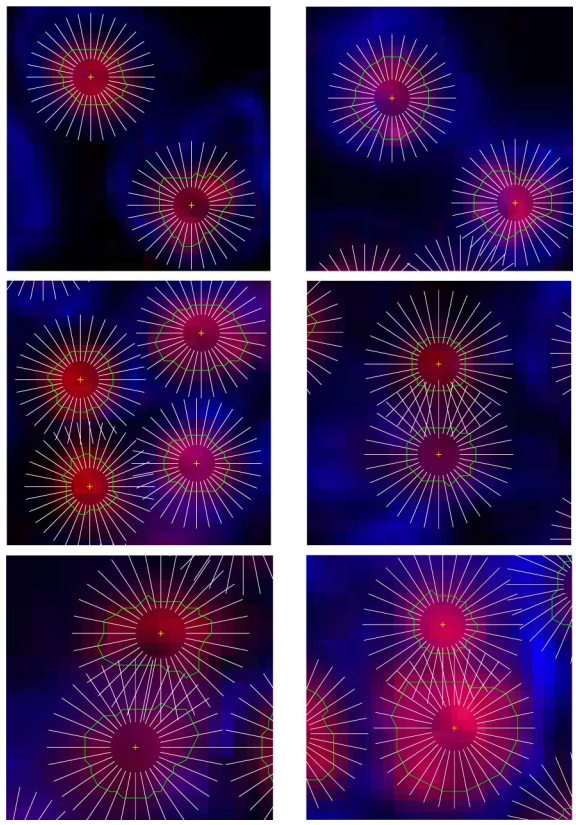

Fig. 6. Examples of SBF nuclei detections with both the central position and the estimated shape overlaid on the original image. In all images the white radial lines range from $R^n_{\min}$ to $R^n_{\max}$. The detected nuclei contours are shown in green.

that contributed to the maximal response that originated that nuclei detection. These are the nuclei band support points $SP^n = \{(x_{SP^n}(\theta_s), y_{SP^n}(\theta_s)), s = 1 \ldots N\}$ which are defined as

$$\begin{aligned} x_{SP^n}(\theta_s) &= x + r^n_{\max}(\theta_s) \times \cos(\theta_s) \\ y_{SP^n}(\theta_s) &= y + r^n_{\max}(\theta_s) \times \sin(\theta_s) \\ r^n_{\max}(\theta_s) &= \underset{R^n_{\min} < r < R^n_{\max}}{\arg\max} \\ &\quad \times \left(\frac{1}{d+1} \sum_{m=r-(d/2)}^{r+(d/2)} CI(s,m) \right) \end{aligned} \tag{3}$$

where N is the number of support region lines, $r^n_{\max}(\theta_s)$ corresponds to the radius in direction θ_s and (x, y) are the detected nuclei center coordinates.

Many cell nuclei detection approaches rely on the Otsu segmentation method [17], or similar methods, to detect cell nuclei in fluorescence images [26]. While less complex this approach cannot handle low contrast nuclei and has the tendency to join clustered nuclei, as shown in Fig. 5(b). Other local operators can also be used to detect cell nuclei, like the Laplacian of Gaussian (LoG) operator. However, this family of methods rely on gradient magnitude (becoming less robust to contrast variations) and cannot properly estimate the cell nuclei shape, as depicted in Fig. 5(d). The result for the SBF filter is also shown in Fig. 5(f) for comparison.

In Fig. 6, we can observe the detected locations and the estimated shapes for several cells. Nuclei detection using the SBF filter performs well even for irregular shapes. Also, even when cells are not clearly separated (bottom row) the filter can still detect each nuclei shape without interference.

To test the SBF robustness to noise we performed detection on degraded images from the simulated dataset, shown in Fig. 7. As can be observed, the proposed approach obtains clear detections and good shape estimations even in images with by high levels of noise [Fig. 7(d)]. Furthermore, the parameters for this test were set for nuclei detection performed on the original image [Fig. 7(b)] and were maintained fixed for the detections on noisy images, further supporting the robustness of our approach.

The use of the SBF filter for the task of cell detection is also supported by previous work where it has been applied to plant nuclei detection in confocal fluorescence microscopy [14], [15] and cancer cell detection in 3-D invasion assays using bright-field microscopy [20].

B. Cell Cytoplasm Shape Estimation

Given the cell nuclei detections we can guide the cytoplasm segmentation by assuming that the approximated convex shape of the cytoplasm has the same convergence center as the corresponding nucleus. This assumption allows us to start the cytoplasm shape estimation from the nuclei's center coordinate and by doing so we are able to discard noisy and irrelevant gradient information. However, the process of estimating the cytoplasm shape support points $SP^c = \{(x_{SP^c}(s), y_{SP^c}(s)), s =$

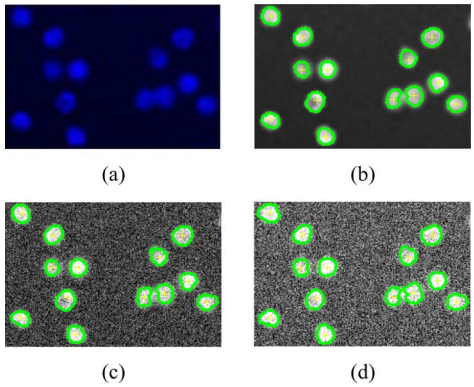

Fig. 7. Cell nuclei detection and shape estimation using the SBF filter, in noisy and low contrast images: (a) Original nuclei image from the simulated dataset, (b) cell nuclei detection, (c) cell nuclei detection after zero mean additive gaussian noise ($\sigma = 0.02$), (d) cell nuclei detection after positive mean additive gaussian noise ($\sigma = 0.04$) (σ^2 is in a unitary scale as specified by MatLab—http://www.mathworks.com/access/helpdesk/help/toolbox/images/imnoise.html).

$1 \ldots N\}$ differs from the one used previously for nuclei shape estimation, and has the following formulation:

$$\begin{aligned} x_{SP^c}(\theta_s) &= x + n^c_{\max}(\theta_s) \times \cos(\theta_s) \\ y_{SP^c}(\theta_s) &= y + n^c_{\max}(\theta_s) \times \sin(\theta_s) \\ r^c_{\max}(\theta_s) &= \underset{R^*_{\min} < r < R^c_{\max}}{\arg\max} \\ &\quad \times \left(\frac{1}{d+1} \sum_{m=r-(d/2)}^{r+(d/2)} CI_{\mathrm{mod}}(s,m) \right) \end{aligned} \tag{4}$$

with

$$CI_{\mathrm{mod}}(s,m) = \cos(\theta_s - \alpha(\theta_s, m)) + k\|grad(\theta_s, m)\|$$

where $R^*_{\min}$ is now the corresponding $r^n_{\max}$ from the nuclei shape estimation for the same radial line s. We add a gradient magnitude term $k\|grad(\theta_s, m)\|$ embedding higher importance to the magnitude of the convergence, according to the weighting factor k. If $k = 0$, (4) simplifies into a similar formulation as (3) which will still estimate the cytoplasm shape and in most cases leads to similar results. However, the magnitude weighting will make it possible to obtain better results in noisy cases (Fig. 8).

By retaining the same (x, y) nuclei central convergence coordinate, the cytoplasm shape estimation process creates a conditioning on the final shape while at the same time selecting the image information to be used in shape estimation. This leads to less possibilities for the cytoplasm shape estimation process to get perturbed by noisy image data.

The restriction that the smaller SBF cytoplasm shape band location, $R^*_{\min}$, must be outside the radius of the nuclei, imposed by $R^*_{\min} > r^n_{\max}$, is intuitive because each nucleus must be inside the respective cell's cytoplasm for a valid cell detection.

Fig. 8 shows the results for the cytoplasm shape estimation where we can see that even in cells with irregular cytoplasm fluorescence the shape estimation is close to the one which would be expected from visual inspection. Additionally, we can observe that overlap between detections occurs, some due to errors and other due to correct detection of real cell overlap. The overlap between cells results from the individual analysis of each cell and the fact that no exclusivity between detections is enforced. However, if desired, different degrees of exclusivity can be enforced allowing the changing of allowed overlap, as we will describe in Sections III-C and III-D.

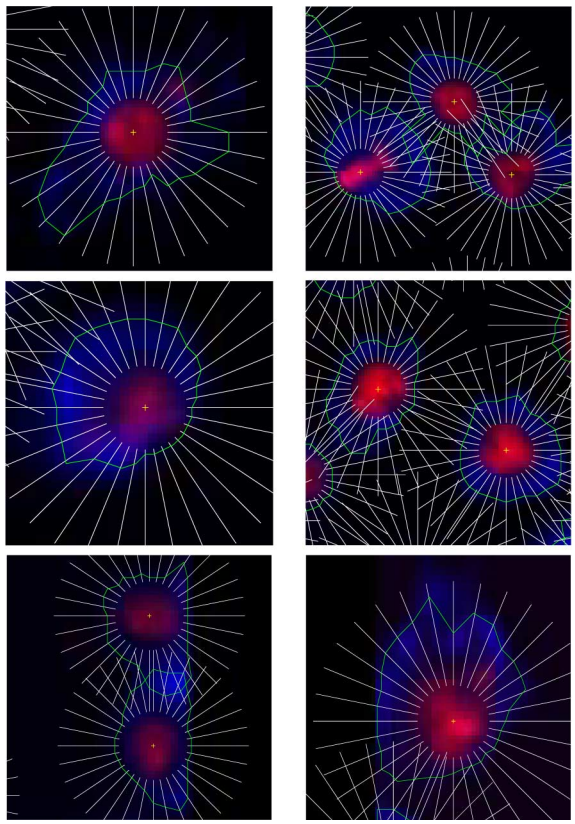

Fig. 8. Cytoplasm shape estimation results (green) with the search radial lines (white). Some overlap can be seen due to captured gradient from other cell's cytoplasm.

C. Cell Detection Validation

The SBF cell detection approach presented in the previous subsections is based on the assumption that the cell's image gradient has a high degree of convergence to the cell's nuclei location. This was the basis of the cell nuclei and cytoplasm shape estimation process. However, this condition was not verified in the cytoplasm shape estimation. As such, to check the validity of the cell detections we now define the total convergence (TC) from both the cell nuclei and cell cytoplasm shapes. The TC for a cell detection is defined as shown in

$$\begin{aligned} \mathrm{TC} = &\frac{1}{N} \sum_{s=1}^{N} \left(\frac{1}{d+1} \sum_{m=r^n_{\max}(\theta_s)-(d/2)}^{r^n_{\max}(\theta_s)+(d/2)} \cos(\theta_s - \alpha(\theta_s, m)) \right) \\ &\times \frac{1}{N} \sum_{s=1}^{N} \left(\frac{1}{d+1} \sum_{m=r^c_{\max}(\theta_s)-(d/2)}^{r^c_{\max}(\theta_s)+(d/2)} \cos(\theta_s - \alpha(\theta_s, m)) \right). \end{aligned} \tag{5}$$

By using the product of the convergence of the nuclei and cytoplasm gradient we assure that the cell detection is only validated when both values of convergence are high. Based on the value of TC, we set a threshold bellow which a cell detection will be discarded as invalid. This gives rise to cell detections which are validated with regards to our assumptions and the image data. In Section III-D we introduced our approach for overlap correction and for the introduction of shape priors.

D. Cell Cytoplasm Overlap Processing

In Section III-C we presented a procedure to validate each detection individually. However, in a group, cell interactions give rise to detections which depend on other cells and may cause the incorrect estimation of cell shape. Overlap is one of those fundamental issues, which can be reduced if we force a minimum distance between detections.

Regarding cytoplasm shape estimation, as mentioned in Section III-B and contrary to segmentation methods, our approach does allow for some cell cytoplasm overlap. While not usual in classic cell detection approaches, this relates to the reality where cells do overlap, as shown in Fig. 8. However, if no cytoplasm shape overlap limitation is imposed errors may occur due to excessive or sometimes complete overlap.

In order to remove badly estimated cell detections we introduce a contour shrinking method that removes overlapping sections of irregular shaped cells. Since some overlap is allowed we select which cells need to suffer shrinking and which do not. This is done by measuring both overlap percentage and irregularity of shape. Shape irregularity is estimated by calculating the cytoplasm shape's average of the squared radial first derivative

$$Irr(SP^c) = \frac{1}{N}\sum_{s=1}^{N}\left(\frac{dr^c_{\max}(\theta_s)}{d\theta_s}\right)^2 \tag{6}$$

where $r^c_{\max}$ is the radius of the cytoplasm shape of the cell detection being analyzed for radial direction θ_s.

For each group of overlapped cells, we process each cell detection starting from the most irregular shape to the most regular one and we calculate the amount of overlap for each cell with all others. If for a cell the overlap is above the allowed threshold, we shrink the respective shape points by moving them radially inwards until the overlap is no longer excessive. Fig. 9 shows several examples of cell detections and the corrections after overlap elimination, where we can observe that cells that do not have enough overlap with other cells are left unchanged.

E. Cell Shape Regularization

As seen in Section III-B applying a convex prior to cell shapes does not enforce a regular rounded shape for the final cell's cytoplasm contour (Fig. 6). Depending on the specific type of cell we are detecting, different amounts of shape smoothness prior may be desired. In order to condition cell cytoplasm shapes to a desired level of compactness, we introduce a radial active contour fitting to the estimated cytoplasm shape that combines radial smoothness and an image energy based on gradient convergence.

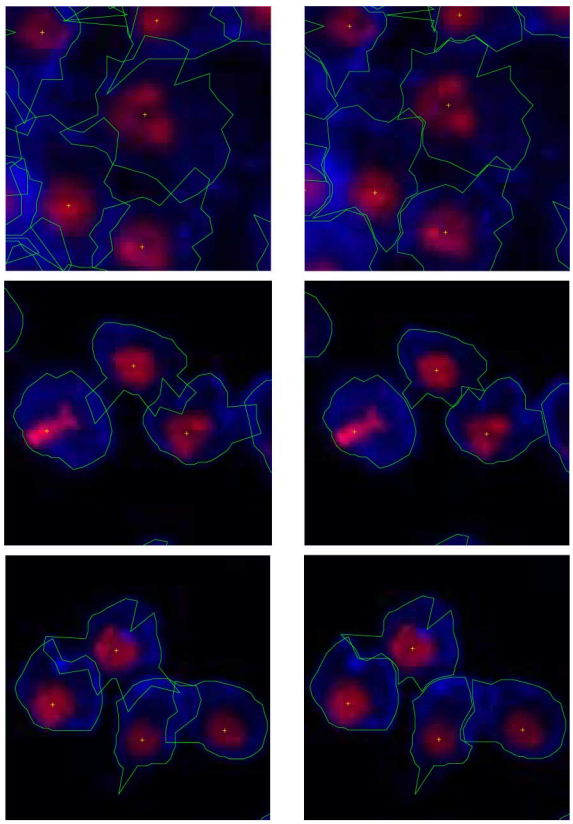

(a) (b)

Fig. 9. Examples of Drosophila cell detections before (left) and after (right) cell cytoplasm overlap correction.

The total energy that governs the cytoplasm shape regularization process is defined by

$$E_{\text{total}}(SP^c) = E_{\text{internal}}(SP^c) + \gamma E_{\text{external}}(SP^c) \tag{7}$$

where γ is a weighting parameter that controls the degree of regularization to better fit the shape smoothness prior or the underlying image convergence.

The shape smoothness energy for the cytoplasm shape $E_{\text{internal}}(SP^c)$ is defined by

$$E_{\text{internal}}(SP^c) = \alpha\left|\frac{dr^c_{\max}(\theta_s)}{d\theta_s}\right|^2 + \beta\left|\frac{dr^c_{\max}(\theta_s)^2}{d\theta_s^2}\right|^2 \tag{8}$$

where α and β are the parameters which control the degree of elasticity and stiffness, respectively, for the cell cytoplasm shape.

The image convergence energy that regulates the fitting of final cell cytoplasm shape to the underlying image information $E_{\text{external}}(SP^c)$ is given by

$$E_{\text{external}}(SP^c) = \frac{1}{N}\sum_{s=1}^{N}\left(\frac{1}{d+1}\sum_{m=r_{\max}(\theta_s)-(d/2)}^{r_{\max}(\theta_s)+(d/2)} CI(s,m)\right). \tag{9}$$

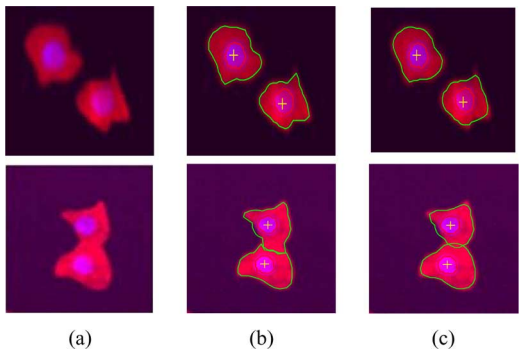

Fig. 10. Cell nuclei and cytoplasm shape estimation examples for the synthetic cell culture image dataset: (a) original images, (b) cell detection after overlap correction, (c) cell detection after shape regularization.

Given the energy formulation in (7) a greedy algorithm is used to minimize the contours energy and obtain a fitted version of the cytoplasm shape.

In contrast with classical active contour formulation there is no constrain energy term that forces the contour to contract or expand. Moreover, such energy term is not necessary as the starting shape is already a good estimation of the cytoplasm shape and not the nuclei shape as used by most active contour methods [2], [25].

Fig. 10 shows the cell nuclei and cytoplasm detections, before and after regularization for the simulated cell culture image dataset. We can observe that for these images the regularization tends to oversimplify the cytoplasmic shape which is highly irregular in this case. This indicates that a shape prior may not be possible to impose for these cells.

In Fig. 11 we can observe the regularized cell cytoplasm estimated shapes for images of the Drosophila Kc167 dataset. Cell shapes before and after regularization are shown in this figure and in this case the regularization process leads to smoother, better fitting contours. We may also notice some correction of singular erroneous points of convergence.

IV. Results and Discussion

In order to test the proposed methodology we present an objective study using several performance measures on both a relatively large dataset of drosophila RNAi multivariate fluorescence microscopy images and an additional simulated cell culture dataset.

A. Parameter Experimental Setting

As discussed in Section III we assume that most parameters of our approach are intuitive and as such do not require validation.

For the Drosophila Kc167 images the following parameters were set based on visual inspection of the cell's shape and size: for the nuclei detection step $R^n_{\min} = 4$, $R^n_{\max} = 14$, for the cytoplasm shape estimation $R^c_{\max} = 35$. Regarding the remaining SBF filter parameters we set $N = 36$ and $q = 5$, where N is a sampling parameter and increases the detected shape smoothness (showing little improvement for values over 36) and q relates to the size of nuclei border gradient and cytoplasmic membrane thickness.

For the simulated cell culture images the following parameters were also set based on visual inspection: for the nuclei detection step $R^n_{\min} = 10$, $R^n_{\max} = 25$, for the cytoplasm shape estimation $R^c_{\max} = 55$. Regarding the remaining SBF filter parameters we set $N = 36$ and $q = 5$.

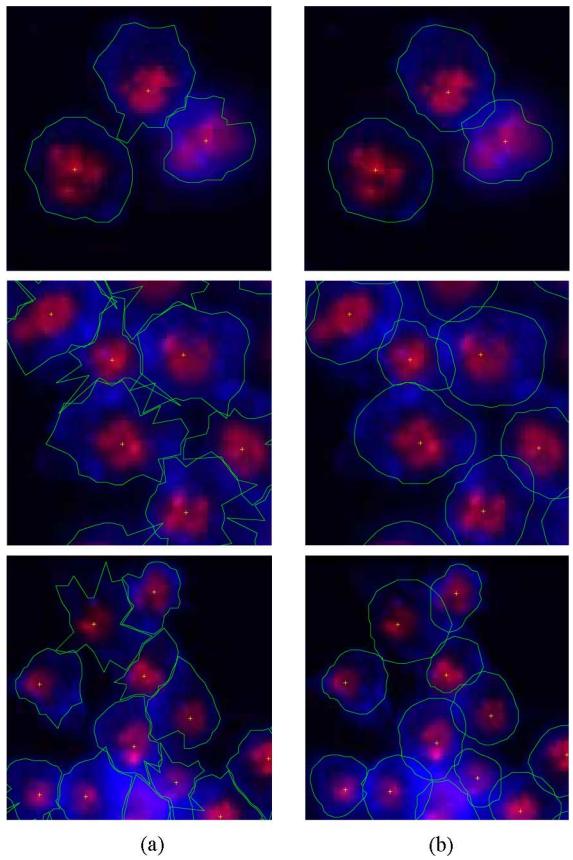

Fig. 11. Examples of the results of cell cytoplasm shape regularization (right) from initially detected shapes (left).

In the experiments for both datasets a minimum distance of $R^n_{\min}$ between detected filter maxima is enforced (allowing for some overlap between tentative nuclei detections). We set this minimum distance equal to the minimum expected radius for the nuclei as it was found to be reasonable during validation.

Regarding all other parameters (overlap threshold, validation threshold and shape energy weights) we used a *k*-fold cross validation, for both datasets, with $k = 4$ leading to different parameter settings and four different test sets.

B. Evaluation Measures

To obtain an objective measure of performance for our cell detection approach we map each detected cell C_j to the best fitting groundtruth region GT_k from the manual segmented image. To obtain this mapping we rely on nuclei information and keep the same mapping for cytoplasm detection performance evaluation. The mapping is obtained using the F_β-score, also known as coverage measure, defined by

$$F_\beta(C_j, GT_k) = \frac{(1+\beta^2)\nu(C_j, GT_k)\rho(C_j, GT_k)}{\nu(C_j, GT_k) + \beta^2\rho(C_j, GT_k)} \quad (10)$$

where ν is precision and ρ is recall, defined by

$$\nu(C_j, GT_k) = \frac{C_j \bigcap GT_k}{C_j}, \quad \rho(C_j, GT_k) = \frac{C_j \bigcap GT_k}{GT_k} \quad (11)$$

TABLE I
CELL DETECTION MEASURES ON THE DROSOPHILA KC167 DATASET. F_β-SCORE, PRECISION, RECALL, AND DETECTION ERROR WERE CALCULATED FOR EACH IMAGE AND AVERAGED OVER THE IMAGES IN THE DATASET. DETECTION PERFORMANCE IS SPLIT BETWEEN NUCLEI DETECTION, CYTOPLASM DETECTION AND CYTOPLASM DETECTION AFTER OVERLAP CORRECTION AND SHAPE REGULARIZATION

	F_1	Precision (%)	Recall (%)	TP	FN	FP
Nuclei detection	80	95	69	67	12	5
Cytoplasm detection	77	67	91	61	15	11
Cytoplasm regularized	89	82	90	64	14	8

and where β is the weighting parameter for the F_β-score. In this paper we use F_1 (i.e., $\beta = 1$) as this is the most common choice for this type of evaluation.

The coverage is evaluated between all pairs of detections and groundtruth, and detections C_j are mapped to GT_k if the F_β-score between them is above a certain threshold th. For the evaluation presented here we consider $th = 0.6$, making it impossible to have multiple groundtruth regions mapped to the same detection.

To provide greater detail on the results' assessment, nuclei and cytoplasm detection are evaluated separately. Given that the process is equal for both fluorescence images, we will consider C_j to be either the cytoplasm or nuclei detection and GT_k the corresponding groundtruth, presenting the evaluation formulation only once.

Based on the mapping between groundtruth and detection we propose two different type of measurements: error counting and shape correctness. Regarding cell detection errors we consider the number of true positive (TP), false positive (FP), and false negative (FN). In the case of shape correctness we compute the F_1-score, precision and recall of estimated shapes in relation to the groundtruth based on (10) and (11).

C. Results

To evaluate the performance of our approach in both real and simulated data we performed a k-fold validation of our approach $(k = 4)$ and calculated the average evaluation measures over the images in all k-folds. We present in Table I the results for the SBF filter applied to nuclei and cytoplasm detection in the Drosophila Kc167 dataset. The results show a precision/recall of 95%/69% for nuclei detection and a precision/recall of 82%/90% for cytoplasm detection, and an overall accuracy of 76%, in the Drosophila Kc167 dataset. Regarding the overlap correction and shape regularization we can see that after applying such methods the performance improves and we obtain fewer false positives. We can also see that nuclei detection has a higher precision and fewer errors overall as expected. While no direct comparison is possible, since neither the used method or dataset is available, these performance numbers are similar to state-of-the-art methods such as in [27]. In Fig. 12, we can qualitatively observe the cell detection results in the Drosophila Kc167 dataset. It can be seen that the groundtruth allows cell shapes which are unlikely to occur and are motivated by segmentation type approaches where overlap is never considered. As expected, cells with a more convex shape and regular cytoplasm are better detected.

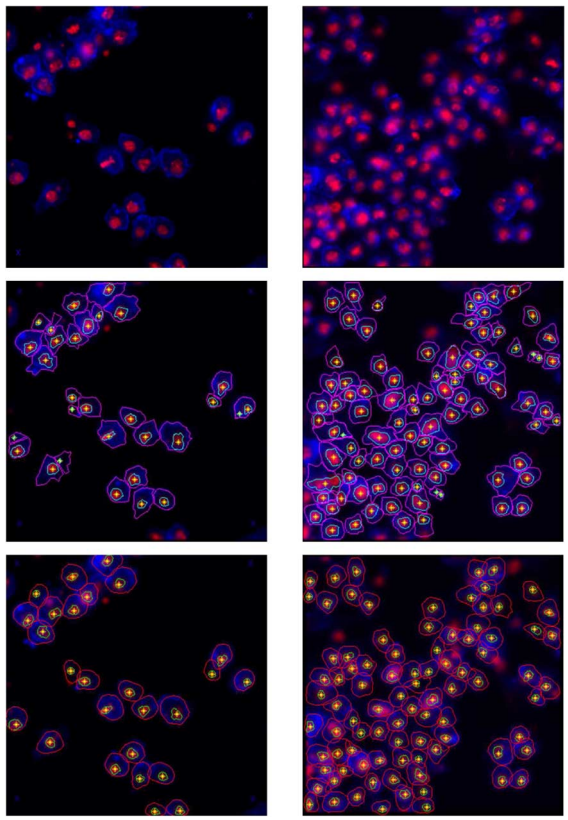

Fig. 12. Results for cell detection for two images of the Drosophila Kc167 dataset. Top: original multivariate images of drosophila cells; middle: available groundtruth; bottom: final cell detection.

TABLE II
CELL DETECTION MEASURES THE SIMULATED CELL CULTURE DATASET. F_β-SCORE, PRECISION, RECALL AND DETECTION ERROR WERE CALCULATED FOR EACH IMAGE AND AVERAGED OVER THE IMAGES IN THE DATASET. DETECTION PERFORMANCE IS SPLIT BETWEEN NUCLEI DETECTION, CYTOPLASM DETECTION AND CYTOPLASM DETECTION AFTER OVERLAP CORRECTION AND SHAPE REGULARIZATION

	F_1	Precision (%)	Recall (%)	TP	FN	FP
Nuclei detection	84	94	74	47	4	4
Cytoplasm detection	86	90	82	44	7	3
Cytoplasm regularized	87	95	80	44	7	3

Additionally, we present in Table II the results for the SBF filter applied to nuclei and cytoplasm detection in the simulated database. Our approach performs better on the simulated dataset with a precision/recall of 94%/74% for nuclei detection and a precision/recall of 95/80% for cytoplasm detection. The better performance in this dataset is mostly due to the higher contrast and overall separation of nuclei, when in comparison to the Drosophila Kc167 dataset (Fig. 13).

D. Results Under the Influence of Noise

To evaluate the behavior of our approach in the presence of noise we performed detection of cells in images from the Drosophila Kc167 dataset after adding Gaussian noise.

For this purpose we randomly selected five images from the Drosophila Kc167 dataset, containing 359 cells, and corrupted each image with zero-mean additive Gaussian noise, with variance ranging from 0.01 to 0.06 (considering pixel intensities

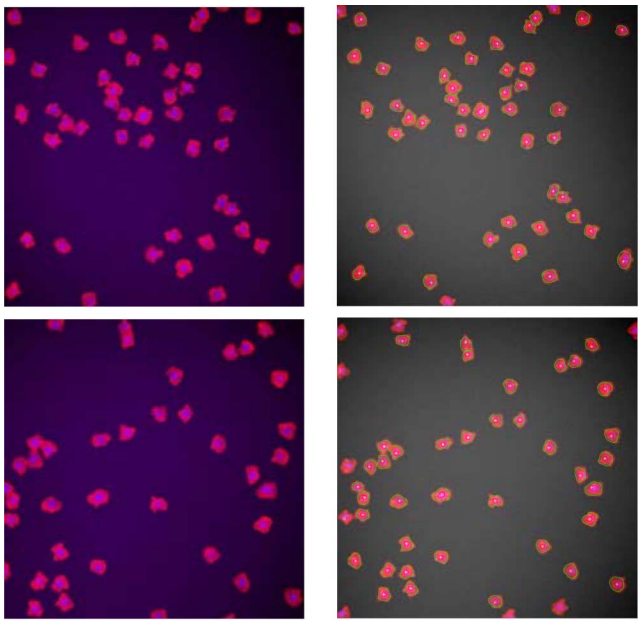

Fig. 13. Results for cell detection for two images of the simulated dataset. Left: original multivariate simulated cell culture images, with color enhancement for better display and printing; right: final cell detection overlaid on the original image.

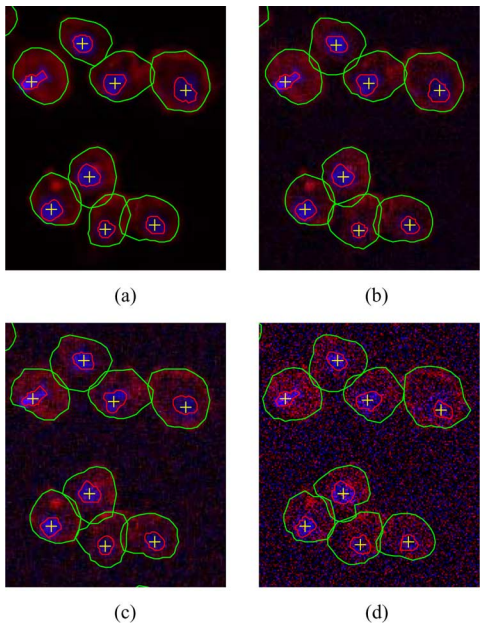

Fig. 14. Detail of cell detection results for images from the Drosophila Kc167 dataset after adding zero mean Gaussian Noise (σ^2 is in a unitary scale as specified by MatLab—http://www.mathworks.com/access/ helpdesk/help/toolbox/images/imnoise.html).

from 0 to 1). Since we aim at testing the robustness of our approach, all parameters were set for the conditions of the original images and not altered for the images after they were affected by noise. Finally, we computed the previously presented error measures for all images and obtained their average values for each noise level.

Fig. 14 shows the cell detection results for images with different levels of added noise. We can see that detections

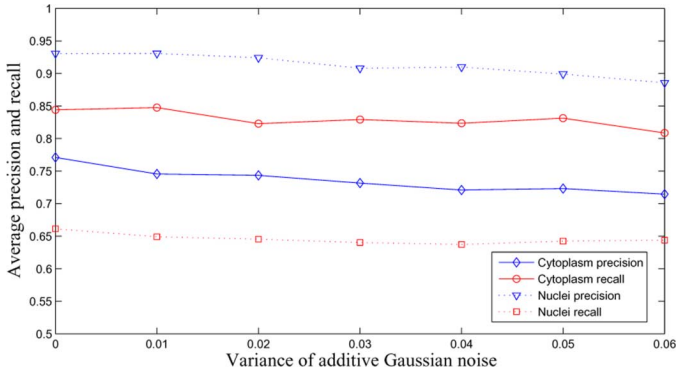

Fig. 15. Noise influence on the average precision and recall for five randomly selected images of the Drosophila Kc167 dataset.

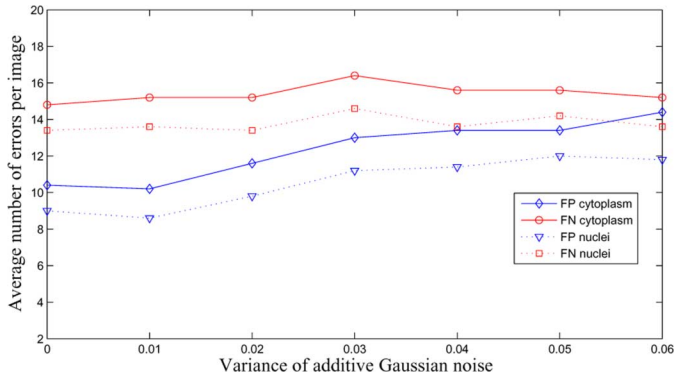

Fig. 16. Noise influence on the average number of false positive (FP) and false negative (FN) for five randomly selected images of the Drosophila Kc167 dataset.

remain considerably stable, even when the noise added leads to an image with little visible information to the human eye.

Figs. 15 and 16 show the performance curves for the measures of cell shape estimation (Precision, Recall) and for detection errors (FP, FN), respectively, for varying noise variance. While the performance of the cell detection approach is reduced with the increase of the variance of the added noise, it never varies more than 10% in the case of precision, recall and false negatives. There is a more significative change in the number of false positives, bellow 10% until $\sigma^2 = 0.02$ but increasing up to 30% for higher values. However, this is due to the fact that the detection threshold should be higher for noisy images.

Regarding computational complexity, our method currently takes 150 s to perform the full segmentation of a 950×950 pixel image on a 3 GHz CPU, with 1 GB of RAM memory. While this is a considerable computationally intensive method, the approach is currently fully implemented in MatLab and could be improved to perform in considerable less time.

V. Conclusion

In this paper, we described a novel approach for cell detection in multivariate fluorescence images which does not rely on image segmentation methods. Instead, the proposed approach is based on local detection by using the SBF gradient convergence filter. Towards cell detection we gather evidence from both nuclei and cytoplasm fluorescence to jointly detect and validate the location of cells and estimate their shapes. Using the

assumption that the cell's cytoplasm convergence center is approximately the same as the corresponding nuclei convergence center we were able to better guide the cytoplasm detection from the nuclei location. Since the SBF is based on convergence this method is robust to contrast variations making it an interesting tool for microscopy fluorescence image analysis. Furthermore, is has the advantage of having intuitive parameters which depend on the physical characteristics of the cell being imaged.

This cell detection method is generic in its nature since it is only based on the principle of convexity of cells. The cell detection problems addressed here are some of the most challenging in current multivariate microscopy image analysis. As such, we believe that it can be applied to other problems of multivariate cell segmentation.

We evaluated our approach for cell detection in a dataset of RNAi images of the Drosophila Kc167, which contain irregular and low contrast cells. The results show a precision/recall of 95%/69% and 82%/90% for nuclei and cytoplasm detection respectively and an overall detection accuracy of 76%.

Further tests also revealed that our approach is robust to noise, maintaining correct detections and adequate shape estimation over a large range of noise.

REFERENCES

[1] A. Bleau and L. Leon, "Watershed-based segmentation and region merging," *Comput. Vis. Image Understand.*, vol. 77, no. 3, pp. 317–370, 2000.

[2] W. Clocksin, "Automatic segmentation of overlapping nuclei with high background variation using robust estimation and flexible contour models," in *Proc. 12th Int. Conf. Image Anal. Process.*, 2003, pp. 682–687.

[3] F. Cloppet and A. Boucher, "Segmentation of overlapping/aggregating nuclei cells in biological images," in *Proc. 19th Int. Conf. Pattern Recognit. (ICPR 2008)*, 2008, pp. 1–4.

[4] O. Danek, P. Matula, C. O. de Solorzano, A. Munoz-Barrutia, M. Maska, and M. Kozubek, "Segmentation of touching cell nuclei using a two-stage graph cut model," in *Proc. SCIA*, 2009, vol. LNCS 5575, pp. 410–419.

[5] Y. Fok, J. Chan, and R. Chin, "Automated analysis of nerve-cell images using active contour models," *IEEE Trans. Med. Imag.*, vol. 15, no. 3, pp. 353–368, Jun. 1996.

[6] N. Harder, F. M-Bermudez, W. Godinez, J. Ellenberg, R. Eils, and K. Rohr, "Automated analysis of mitotic cell nuclei in 3-D fluorescence microscopy image sequences," in *Workshop Bio-Image Inf.: Biol. Imag., Comput. Vis. Data Mining*, Santa Barbara, CA, 2008, pp. 17–18.

[7] A. Hill, P. LaPan, Y. Li, and S. Haney, "Impact of image segmentation on high-content screening data quality for sk-br-3 cells," *BMC Bioinformatics*, vol. 8, no. 340, pp. 1–13, 2007.

[8] M. Hu, X. Ping, and Y. Ding, "A new active contour model and its application on cell segmentation," in *Proc. Control, Automat., Robot. Vis. Conf. (ICARCV)*, 2004, vol. 2, pp. 1104–1107.

[9] T. R. Jones, A. Carpenter, and P. Golland, "Voronoi-based segmentation of cells on image manifolds," in *ICCV Workshop Comput. Vis. Biomed. Image Appl. (CVBIA)*, 2005, pp. 535–543.

[10] A. Klemencic, S. Kovacic, and F. Pernus, "Automated segmentation of muscle fiber images using active contour models," *Cytometry*, vol. 32, pp. 317–326, 1998.

[11] H. Kobatake and S. Hashimoto, "Convergence index filter for vector fields," *IEEE Trans. Image Process.*, vol. 8, no. 8, pp. 1029–1038, Aug. 1999.

[12] A. Lehmussola, P. Ruusuvuori, J. Selinummi, H. Huttunen, and O. Yli-Harja, "Computational framework for simulating fluorescence microscope images with cell populations," *IEEE Trans. Med. Imag.*, vol. 26, no. 7, pp. 1010–1016, Jul. 2007.

[13] V. Luc and P. Soille, "Watersheds in digital spaces: An efficient algorithm based on immersion simulations," *IEEE Trans. Pattern Anal. Mach. Intell.*, vol. 13, no. 6, pp. 583–598, Jun. 1991.

[14] M. Marcuzzo, T. Guichard, P. Quelhas, A. M. Mendonça, and A. Campilho, "Cell division detection on the arabidopsis thaliana root," in *Proceedings of IbPRIA*. New York: Springer, 2009, vol. 5524, LNCS, pp. 168–175.

[15] M. Marcuzzo, P. Quelhas, A. M. Mendonça, and A. Campilho, "Evaluation of symmetry enhanced sliding band filter for plant cell nuclei detection in low contrast noisy fluorescent images," in *Proceedings of ICIAR*. New York: Springer, 2009, vol. 5627, LNCS, pp. 824–831.

[16] P. Moore and D. Molloy, "A survey of computer-based deformable models," in *Int. Mach. Vis. Image Process. Conf. (IMVIP)*, 2007, pp. 55–66.

[17] N. Otsu, "A threshold selection method from gray-level histograms," *IEEE Tran. Syst., Man, Cybern.*, vol. 9, no. 1, pp. 62–66, Jan. 1979.

[18] C. S. Pereira, H. Fernandes, A. M. Mendonça, and A. Campilho, "Detection of lung nodule candidates in chest radiographs," *LNCS*, vol. 4478, pp. 170–177, 2007.

[19] C. S. Pereira, A. M. Mendonça, and A. Campilho, "Evaluation of contrast enhancement filters for lung nodule detection," in *Proceedings of ICIAR*. New York: Springer, vol. 4633, pp. 878–888.

[20] P. Quelhas, M. Marcuzzo, M. J. Oliveira, A. M. Mendonça, and A. Campilho, "Cancer cell detection and invasion depth estimation in brightfield images," in *Proc. 20th Br. Mach. Vis. Conf. (BMVC)*, London, U.K., 2009.

[21] P. Ruusuvuori, A. Lehmussola, J. Selinummi, T. Rajala, H. Huttunen, and O. Yli-Harja, "Benchmark set of synthetic images for validating cell image analysis algorithms," in *Proc. 16th Eur. Signal Process. Conf.*, Lausanne, Switzerland, 2008.

[22] C. Solorzano, R. Malladi, S. Lelievre, and S. Lockett, "Segmentation of nuclei and cells using membrane related protein markers," *J. Microscopy*, vol. 201, pp. 404–415, 2001.

[23] F. B. Tek, A. G. Dempster, and I. Kale, *Mathematical Morphology: 40 Years On*. New York: Springer, 2006, vol. 30, pp. 441–454.

[24] J. Wei, Y. Hagihara, and H. Kobatake, "Detection of rounded opacities on chest radiographs using convergence index filter," in *Proc. Int. Conf. Image Anal. Process.*, 1999, pp. 757–761.

[25] G. Xiong, X. Zhou, L. Ji, P. Bradley, N. Perrimon, and S. Wong, "Segmentation of drosophila RNAI fluorescence images using level sets," in *Proc. IEEE Int. Conf. Image Process.*, 2006, pp. 73–76.

[26] G. Xiong, X. Zhou, and L. Ji, "Automated segmentation of drosophila RNAi fluorescence cellular images using deformable models," *IEEE Trans. Circ. Syst. I*, vol. 53, no. 11, pp. 2415–2424, Nov. 2006.

[27] P. Yan, X. Zhou, M. Shah, and S. T. C. Wong, "Automatic segmentation of high-throughput RNAi fluorescent cellular images," *IEEE Trans. Inf. Technol. Biomed.*, vol. 12, no. 1, pp. 109–117, Jan. 2008.

[28] X. Yang, H. Li, and X. Zhou, "Nuclei segmentation using marker-controlled watershed, tracking using mean-shift, and kalman filter in time-lapse microscopy," *IEEE Trans. Circuits Syst.*, vol. 53, no. 11, pp. 2405–2414, Nov. 2006.